Climb of jogs as a rate-limiting process of screw dislocations motion in olivine dislocation creep

Lin Wang[a, b] and Tomoo Katsura[a, c]

[a] Bayerisches Geoinstitut, University of Bayreuth, 95440 Bayreuth, Germany.

[b] Geophysical laboratory, Carnegie institution for Science, Washington D.C., 20015, U.S.A.

[c] Center for High Pressure Science and Technology Advanced Research, Beijing, 100094, China

* Corresponding author.

E-mail address: liwang@carnegiescience.edu

Abstract

Dislocation recovery experiments were conducted on pre-deformed olivine single crystals at temperatures of 1,450 to 1,760 K, room pressure, and oxygen partial pressures near the Ni-NiO buffer to determine the annihilation rates constants for [001] (010) edge dislocations. The obtained rate constants were comparable with those of previously determined [001] screw dislocations. The activation energies for the motion of both dislocations are identical. This suggests that the motion of screw dislocations in olivine is not controlled by cross-slip but by the same rate-limiting process of the motion of edge dislocations, i.e. climb, at low-stress and high-temperature conditions. The diffusivity derived from dislocation climb indicates that dislocation recovery is controlled by pipe diffusion. The conventional climb controlled model for olivine can be applied to the motions of not only edge but also screw dislocations. The softness of the asthenosphere cannot be explained by the cross-slip controlled olivine dislocation creep.

Keywords: dislocation recovery, dislocation creep, temperature dependence, climb controlled model, asthenosphere

Introduction

Geophysical observations regarding geoid (e.g. Hager, 1991) and post-glacial rebound (e.g. Peltier, 1998) suggested that a soft asthenosphere underlies a rigid lithosphere. Geodynamic modellings (e.g. Becker, 2017; Craig and McKenzie, 1986) also suggested the same conclusion. The reason for the soft asthenosphere is under debate. Although the simplest explanation is weakening of materials due to the high temperature, results of deformation experiments on dry peridotite implied that the high temperatures are insufficient to explain the softness of asthenosphere (Hirth and

Kohlstedt, 2003). Although a popular explanation is hydrous weakening of olivine (e.g. Mackwell et al., 1985; Hirth and Kohlstedt, 2003), it is doubted by recent Si self-diffusion experiments (Fei et al., 2016; Fei et al., 2013) based on the assumption that dislocation creep is controlled by diffusion. Another possible explanation was proposed by Poirier and Vergobbi (1978). They suggested that, if cross-slip of dissociated screw dislocations controls olivine dislocation creep, the estimated upper-mantle viscosity would be one order of magnitude lower than that predicted by the climb controlled model in the stress range from 10 to 100 bar. This potentially explains the softness of the asthenosphere. However, there is no experimental study to test this hypothesis.

Neither diffusion nor deformation experiments can identify the rate-limiting process of motions of screw dislocations. Diffusion does not involve motions of dislocations. Although it is theoretically possible to determine the rate-limiting process of dislocation motions by examining the stress dependence of creep rates (e.g. Hirth and Kohlstedt, 2003), the stress ranges in deformation experiments are too narrow. Conventionally used stress exponent of 3.5 for dislocation creep implies a pipe diffusion controlled mechanism (Hirth and Kohlstedt, 2003, 2015). However, those experiments have a stress range only from 100 to 224 MPa. On the other hand, Kohlstedt and Goetze (1974) found that stress exponent increases with increasing stress. Poirier (1985, P.139) found that the stress exponent of olivine single crystal dislocation creep varies from 2.6 to 3.7 in different studies.

In this study, we conducted dislocation recovery experiments on [001](010) edge dislocations and compared the results with those of [001](010) screw dislocations from Wang et al. (2016). During recovery, dislocations move on the slip plane (glide) and out of the slip plane (climb, cross-slip) successively under the influence of internal stress. Therefore, the activation energy determined by this method represents that of the rate-limiting process of dislocation motions. Although the model

from Poirier and Vergobbi (1978) was based on [100] screw dislocations, most of them have edge character at temperature less than 1350 ºC (Bai and Kohlstedt, 1992; Wang et al., 2016). On the other hand, the similar density of edge and screw dislocations in [001](010) slip system (Wang et al., 2016) indicates equivalent importance of both types of dislocations in this slip system. Therefore, we focus on this slip system in this study (here after called ***c***-dislocations).

Experimental Procedure

The same Pakistan olivine and sample preparation procedure as those of Wang et al. (2016) were employed in this study. The composition of olivine was reported by Gose et al. (2010). The experimental setup is similar with that in Wang et al. (2016). The olivine single crystal was orientated by X-ray diffraction and electron backscattered diffraction (EBSD), and then placed in the cell assembly such that the [001] direction and (010) plan are parallel to the shear direction and plane, respectively.

Dislocations with the [001] Burgers vector on the (010) plane were produced by experimental deformation using a Kawai-type multi-anvil apparatus at University of Bayreuth. The sample assembly was first pressurized to 3 GPa with a press load of 3.6 MN, and then heated to a temperature of 1,600 K and held for 15 min to sinter crushable alumina. After that, the assembly was further compressed to a press load of 3.9 MN for 15 min to deform the sample. After the deformation, the sample was quenched by switching off the heating power, and then decompressed to room pressure for more than 16 hours. Transmission electronic microscopy (TEM) by Wang et al. (2016) found [001](010) slip system was successfully activated and dominant by this procedure. The ratio of screw to edge dislocations was 3:2, as reported by Wang et al. (2016).

The deformed olivine crystals were cut into eight cubic pieces, and paired into four groups, in which the two pieces in each group shared a common (100) plane. One piece from each pair was used to determine the initial dislocation density, while the other was used to determine dislocation density after the annealing. The annealing experiments were conducted at ambient pressure and temperatures of 1,460 to 1,760 K for 35 min to 24 hours using a gas mixing furnace. The oxygen partial pressure was controlled at 10^{-6}-10^{-8} MPa, which is near the Ni-NiO buffer, using a CO-CO_2 gas mixture. Table 1 summarizes conditions of the annealing experiments.

Dislocations were observed using oxidation decoration technique (Kohlstedt et al., 1976, Karato 1987). The corresponding areas away from sub-grain boundaries on the common (100) plane in the initial and annealed pieces from the same group were observed to determine the change in dislocation densities before and after annealing. Since [001](010) edge dislocations elongate in [100] direction, these dislocations show dots contrast on (100) plane in backscattered images after decoration. The dots per unit area were counted as the dislocation density.

The annihilation rate constants were calculated using the second-order dislocation recovery kinetics (Karato and Ogawa, 1982; Kohlstedt et al., 1980; Wang et al., 2016)

$$k = \frac{\frac{1}{\rho_f} - \frac{1}{\rho_i}}{t}, \quad (2)$$

where ρ_f and ρ_i are the dislocation densities after and before annealing, respectively, and t is the annealing time. Because of the thermally activated process, the dislocation annihilation rate constant is assumed to follow the Arrhenius relationship:

$$k = k_0 \exp\left(-\frac{E}{RT}\right) \quad (3)$$

where k_0 is a constant, E is the activation energy of dislocation annihilation, T is the temperature, and R is the gas constant.

Results

Table 1 shows experimental results together with the annealing conditions. Dislocation density in the samples before deformation is less than 0.0004 μm^{-2}, which is negligible in comparison with dislocation density after deformation (Table 1). Figure 1 a and b shows back-scattered electron images of decorated dislocations in the corresponding areas in the samples from the same pair before and after annealing, respectively. The ***c***-screw dislocations appear as lines and the ***c***-edge dislocations as dots on the (100) plane due to their geometries. Decrease in dislocation density was observed by comparing the images before and after annealing. The water contents in the samples before and after annealing were below the detection limit of infrared spectroscopy. The transmission electron microscope images of the dislocation structures after deformation were given in Fig. 4 in Wang et al. (2016).

Figure 1c plots the logarithmic rate constants of ***c***-edge dislocations annihilation against the reciprocal temperature. The results from the previous dislocation recovery experiments on *c*-screw dislocations (Wang et al., 2016) and from other studies on dislocation recovery kinetics are also plotted in this figure. The dislocation annihilation rate constants of ***c***-edge and ***c***-screw dislocations are comparable, but those of the ***c***-screw are about half orders of magnitude higher than those of the ***c***-edge. The temperature dependences for these two dislocations are identical. Their activation energies are $E_{\text{c-edge}}$ = 400 ± 20 kJ/mol and $E_{\text{c-screw}}$ = 400 ± 30 kJ/mol for the ***c***-edge and ***c***-screw, respectively.

Discussion

The identical activation energies of annihilation rate constants of the ***c***-edge and ***c***-screw dislocations indicate that the motions of both dislocations are controlled by the same mechanism. Although many transport properties of olivine exhibit activation energies between 300 to 500 kJ/mol (e.g. Dohmen et al., 2002, 529 ± 41 kJ/mol for silicon self diffusion, 338 ± 14 kJ/mol for oxygen self diffusion), they are distinct from those determined in this study (also see the slope in Fig.3 and references there). The high accuracy in activation energies obtained in previous and this study allows us to distinguish the rate-limiting mechanisms of different processes.

The motion of edge dislocations is controlled by climb at high temperatures and low stresses (e.g. Hull and Bacon, 2001; Kohlstedt, 2006). However, motion of a pure screw dislocation does not involve climb because screw segments have no specific slip plane (Hull and Bacon, 2001). Since jogs in screw dislocations has edge character, we propose that the motion of screw dislocation is controlled by climb of jogs (Fig. 2). A screw dislocation can form a jog by cross-slips to overcome obstacles that it meets during glide (Fig.2A and 2B). The slip plane of the jog is defined by its dislocation line (***J***) and the Burgers vector (***b***), indicated by the yellow plane. The parent screw dislocation glides in the *y* direction and therefore, the jog needs to climb in the *y* direction to move along with their parental dislocation so that the screw dislocation can go through the obstacle (Fig. 2C). This climb of jogs should serve as the rate-limiting process of the screw dislocation motions.

It is noted that although the climb of edge dislocation and jog motion of screw dislocation are essentially the same, the density of climbing parts on edge dislocations and that of jogs on screw dislocations may be different, which causes difference in magnitude of rate constants. Thus, only the slope in the Arrhenius plot can be a fingerprint of the essential mechanism of rate-limiting processes in dislocation recovery experiments.

Since climb is controlled by diffusion, the diffusivities derived from annihilation rate constants, D^R (based on Karato and Ogawan, 1989) were compared with those of silicon and oxygen diffusion in olivine (Fig. 3). None of these data fit D^R well. Instead, D^R fall between silicon lattice and grain boundary diffusivities. This indicates that the dislocation climb in olivine may be controlled by pipe diffusion. Vacancies, dislocations and grain boundaries are 0-, 1-, 2-dimension defects, the structure distortion near these defects should increase consequently and accordingly, the associated Si diffusivity should increase consequently. In addition, the activation energy of D^R obtained in this study is between those of Si lattice (540 kJ/mol, Dohmen et al., 2002) and grain boundary diffusion (~200 kJ/mol, Fei et al., 2015). This is also consistent with the hypothesis that pipe diffusion controls dislocation climb. Although there is no data for the pipe diffusion in olivine, the fact that diffusion coefficient and activation energy of pipe diffusion are between those of lattice and grain boundary diffusion are well established in oxides (Frost and Ashby, 1983, Table 12.1). The low activation energy of oxygen lattice diffusion (~340 kJ/mol, Dohmen et al., 2002) rules out the possibility that oxygen diffusion controls dislocation climb.

Implications

It was proposed that the softness of asthenosphere can be explained by the cross-slip controlled dislocation creep of olivine (Poirier and Vergobbi, 1978). However, this hypothesis was never tested. The present study demonstrates that motion of [001] screw dislocations is controlled by climb of jogs rather than cross-slip, suggesting that cross-slip model is not applicable for such dislocations in olivine. Although the cross-slip model is based on [100] dislocations, study of [001](010) slip system is more relevant to the asthenosphere conditions. Dislocation structure analyses indicated that most

[100](010) dislocations have edge character (Bai and Kohlstedt, 1992, Wang et al., 2016), indicating that olivine dislocation creep cannot be controlled by the motions of [100] screw dislocation. On the other hand, the similar density (Wang et al., 2016) of edge and screw dislocations in [001](010) slip system indicates that both kinds of dislocations are important. Moreover, deformation experiments (e.g. Raterron et al., 2007) suggested that this slip system dominated at high pressure. Therefore, we conclude that cross-slip of screw dislocations cannot control the dislocation creep of olivine and accordingly, it cannot explain the softness of asthenosphere. The climb controlled model can be used in olivine dislocation creep regardless of dislocation characters.

The viscosity of asthenosphere extrapolated from dry olivine creep data using climb model is orders of magnitude higher than the estimated value from geophysical observation (Hirth and Kohlstedt 2003). Hydrous weakening of olivine was proposed to explain this discrepancy (e.g. Mackwell et al., 1985; Hirth and Kohlstedt, 2003) but it was disparaged by recent Si diffusion experiments (Fei et al., 2016; Fei et al., 2013). However, this study indicates that pipe diffusion, rather than lattice or grain boundary diffusion, may control the dislocation motions. This may explain the discrepant results between deformation and diffusion experiments. Further studies on the effect of water on the dislocation recovery or pipe diffusion in olivine are needed to identify the effect of water on the olivine rheology and to better explain the softness of the asthenosphere.

Acknowledgements

We thank H. Fischer, R. Njul in BGI for the sample and assembly preparation. This research was supported by DFG grants to TK (KA3434-3/1, KA3434-3/2, KA3434-7/1 and KA3434-8/1) and by the annual budget of BGI. All data used in this paper are in Table 1 and plotted in Figure. 1c

192 **Reference**

193 Bai, Q., and Kohlstedt, D. L., 1992, High-temperature creep of olivine single crystals, 2. dislocation
194 structures: Tectonophysics, v. 206, no. 1–2, p. 1-29.
195 Becker, T. W., 2017, Superweak asthenosphere in light of upper mantle seismic anisotropy:
196 Geochemistry, Geophysics, Geosystems.
197 Craig, C. H., and McKenzie, D., 1986, The existence of a thin low-viscosity layer beneath the
198 lithosphere: Earth and Planetary Science Letters, v. 78, no. 4, p. 420-426.
199 Dohmen, R., Chakraborty, S., and Becker, H.-W. (2002) Si and O diffusion in olivine and implications
200 for characterizing plastic flow in the mantle. Geophysical Research Letters, 29(21), 2030.
201 Farver, J.R., and Yund, R.A. (2000) Silicon diffusion in forsterite aggregates: Implications for
202 diffusion accommodated creep. Geophysical Research Letters, 27(15), 2337-2340.
203 Fei, H., Koizumi, S., Sakamoto, N., Hashiguchi, M., Yurimoto, H., Marquardt, K., Miyajima, N.,
204 Yamazaki, D., and Katsura, T., 2016, New constraints on upper mantle creep mechanism
205 inferred from silicon grain-boundary diffusion rates: Earth and Planetary Science Letters, v.
206 433, p. 350-359.
207 Fei, H., Wiedenbeck, M., Yamazaki, D., and Katsura, T., 2013, Small effect of water on upper-mantle
208 rheology based on silicon self-diffusion coefficients: Nature, v. 498, no. 7453, p. 213.
209 Frost, H.J. and M.F. Ashby, Deformation mechanism maps: the plasticity and creep of metals and
210 ceramics. 1982: Pergamon press.
211 Gose, J., Schmaedicke, E., Markowitz, M., and Beran, A., 2010, OH point defects in olivine from
212 Pakistan: Mineralogy and Petrology, v. 99, no. 1-2, p. 105-111.
213 Hager, B. H., 1991, Mantle viscosity: A comparison of models from postglacial rebound and from the
214 geoid, plate driving forces, and advected heat flux, Glacial isostasy, sea-level and mantle
215 rheology, Springer, p. 493-513.
216 Hirth, G., and Kohlstedt, D., 2003, Rheology of the Upper Mantle and the Mantle Wedge: A View
217 from the Experimentalists, Inside the Subduction Factory, American Geophysical Union, p.
218 83-105.
219 Hirth, G., and Kohlstedt, D., 2015, The stress dependence of olivine creep rate: Implications for
220 extrapolation of lab data and interpretation of recrystallized grain size: Earth and Planetary
221 Science Letters, v. 418, p. 20-26.
222 Hull, D., and Bacon, D. J., 2001, Introduction to dislocations, Butterworth-Heinemann. P.257
223 Karato, S., and Ogawa, M., 1982, High-pressure recovery of olivine: implications for creep
224 mechanisms and creep activation volume: Physics of the Earth and Planetary Interiors, v. 28,
225 no. 2, p. 102-117.
226 Karato, S., Scanning electron microscope observation of dislocations in olivine. Physics and
227 Chemistry of Minerals, 1987. 14(3): p. 245-248.
228 Kohlstedt, D.L., et al., New Technique for Decorating Dislocations in Olivine. Science, 1976.
229 191(4231): p. 1045-1046.
230 Kohlstedt, D., Nichols, H., and Hornack, P., 1980, The effect of pressure on the rate of dislocation
231 recovery in olivine: Journal of Geophysical Research: Solid Earth (1978–2012), v. 85, no. B6,
232 p. 3122-3130.
233
234 Kohlstedt, D. L., 2006, The Role of Water in High-Temperature Rock Deformation: Reviews in
235 Mineralogy and Geochemistry, v. 62, no. 1, p. 377-396.

Kohlstedt, D. L., and Goetze, C., 1974, Low-stress high-temperature creep in olivine single crystals: Journal of Geophysical Research, v. 79, no. 14, p. 2045-2051.

Mackwell, S.J., Kohlstedt, D.L., and Paterson, M.S. (1985) The role of water in the deformation of olivine single-crystals. Journal of Geophysical Research-Solid Earth and Planets, 90(NB13), 1319-1333.Peltier, W., 1998, Postglacial variations in the level of the sea: Implications for climate dynamics and solid‐earth geophysics: Reviews of Geophysics, v. 36, no. 4, p. 603-689.

Poirier, J.-P., 1985, Creep of crystals: high-temperature deformation processes in metals, ceramics and minerals, Cambridge University Press.

Poirier, J.-P., and Vergobbi, B., 1978, Splitting of dislocations in olivine, cross-slip-controlled creep and mantle rheology: Physics of the Earth and Planetary Interiors, v. 16, no. 4, p. 370-378.

Raterron, P., Chen, J., Li, L., Weidner, D., and Cordier, P. (2007) Pressure-induced slip-system transition in forsterite: Single-crystal rheological properties at mantle pressure and temperature. American Mineralogist, 92(8-9), 1436-1445.

Wang, L., Blaha, S., Pintér, Z., Farla, R., Kawazoe, T., Miyajima, N., Michibayashi, K., and Katsura, T., 2016, Temperature dependence of [100](010) and [001](010) dislocation mobility in natural olivine: Earth and Planetary Science Letters, v. 441, p. 81-90.

Weertman, J., 1955, Theory of Steady‐State Creep Based on Dislocation Climb: Journal of Applied Physics, v. 26, no. 10, p. 1213-1217.

Figure and table captions

Figure 1. BEIs showing the dislocation density (a) before and (b) after annealing at 1760 K for 35 minutes. The images were taken on the (100) plane. Screw and edge dislocations are lines and dots, respectively, due to the geometries of their dislocation lines. The yellow scale bar represents 2 μm. (c) Logarithmic dislocation annihilation rate constants of ***c***-edge dislocations versus reciprocal temperature. Together plotted are the annihilation rate constants of ***c***-screw dislocations from Wang et al., (2016). The activation energies for both dislocations are identical, i.e. 400 kJ/mol. Previous results on dislocation recovery are also plotted for comparison.

Figure 2. A schematic diagram showing the jog-climb controlled motion of a screw dislocation. (a) The screw dislocation (blue line) is elongated in the *x* direction, which is parallel to its Burgers vector ***b***, and glides in the *y* direction. The blue dot represents the obstacle that the screw dislocation meets during glide. (b) A jog (red segment) elongated in the *z* direction is produced on the screw dislocation in order to overcome the obstacle. This jog has an edge nature with the same Burgers vector ***b*** as the parental screw dislocation. The yellow area indicates the glide plane of the jog, which is normal to the *y* direction. (c) The jog has to climb out of its glide plane in order to move along with its parental screw dislocation.

Figure 3. Logarithmic diffusivity derived from dislocation annihilation rate constants of ***c***-edge and ***c***-screw dislocations versus reciprocal temperature. Together plotted are Si and O lattice and grainboundary diffusivities.

Table 1. Summary of experiment conditions and results.

Table 1. Summary of experimental conditions and results*.

[001](010) edge dislocation						
Sample	*T* (K)	Annealing time (h)	log(f_{O_2}, 10^5 Pa)	ρ_i (μm^{-2})	ρ_f (μm^{-2})	log(k, m^{2}s^{-1})
Z1643-1	1763	0.58	-4.9	1.60±0.13	0.29±0.01	-14.87±0.03
				0.97±0.13	0.22±0.01	-14.77±0.03
Z1643-2	1673	2.5	-5.7	1.49±0.04	0.36±0.06	-15.63±0.09
				1.13±0.12	0.31±0.03	-15.58±0.05
Z1643-3	1473	24	-7.7	1.33±0.15	0.73±0.05	-17.14±0.09
				0.35±0.03	0.29±0.01	-17.22±0.27

* different ρ_i and ρ_f in each sample correspond to different areas

286 Figure 1.

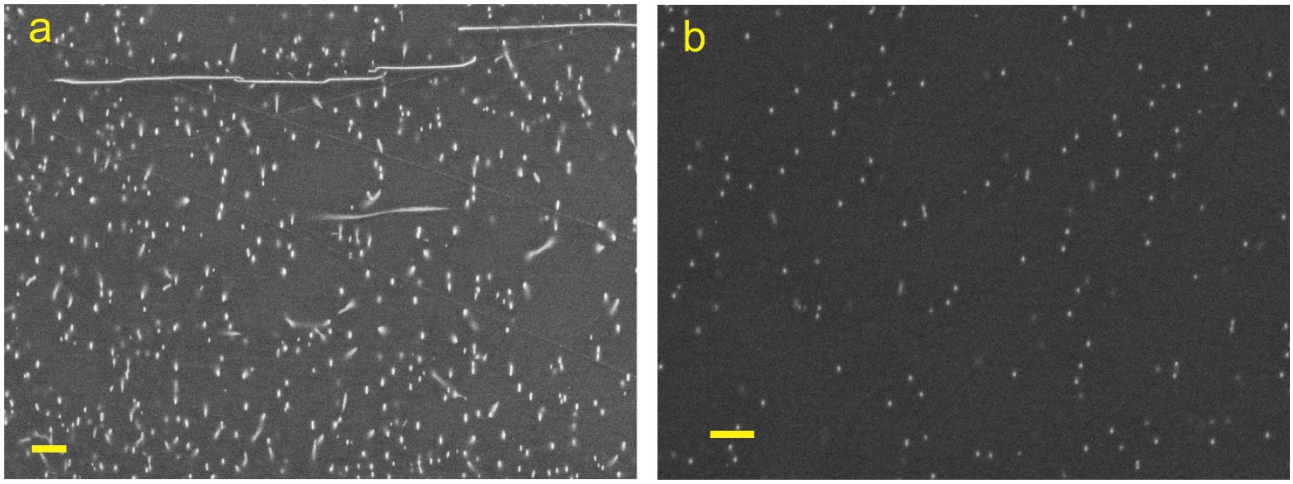

287

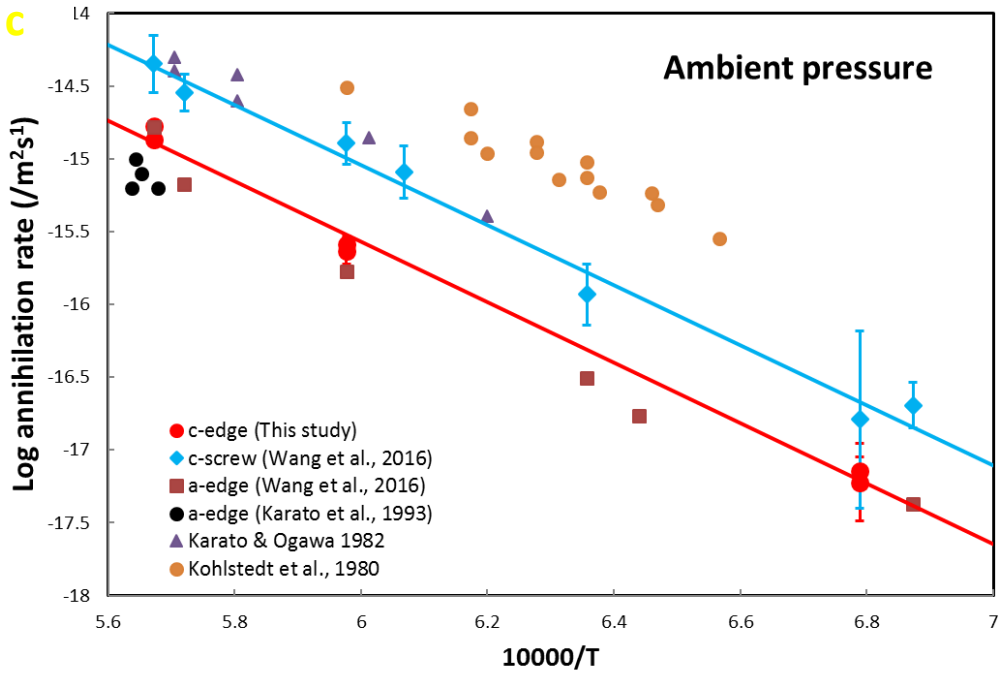

288

289

290

291 Figure 2.

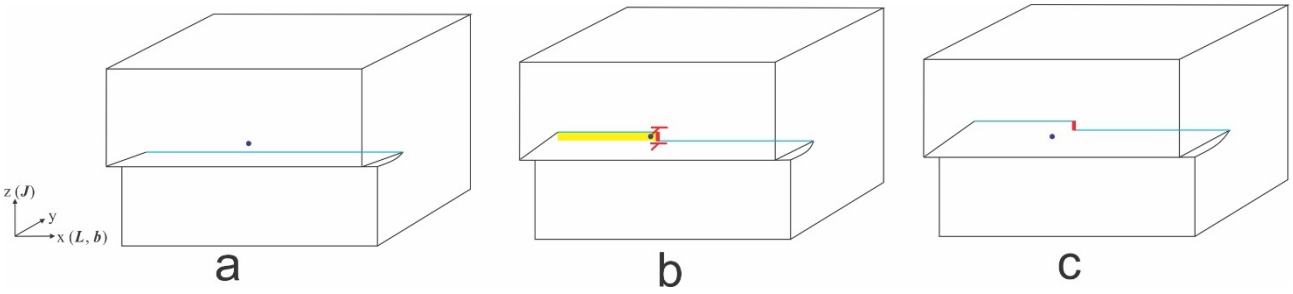

292

293

294 Figure 3.

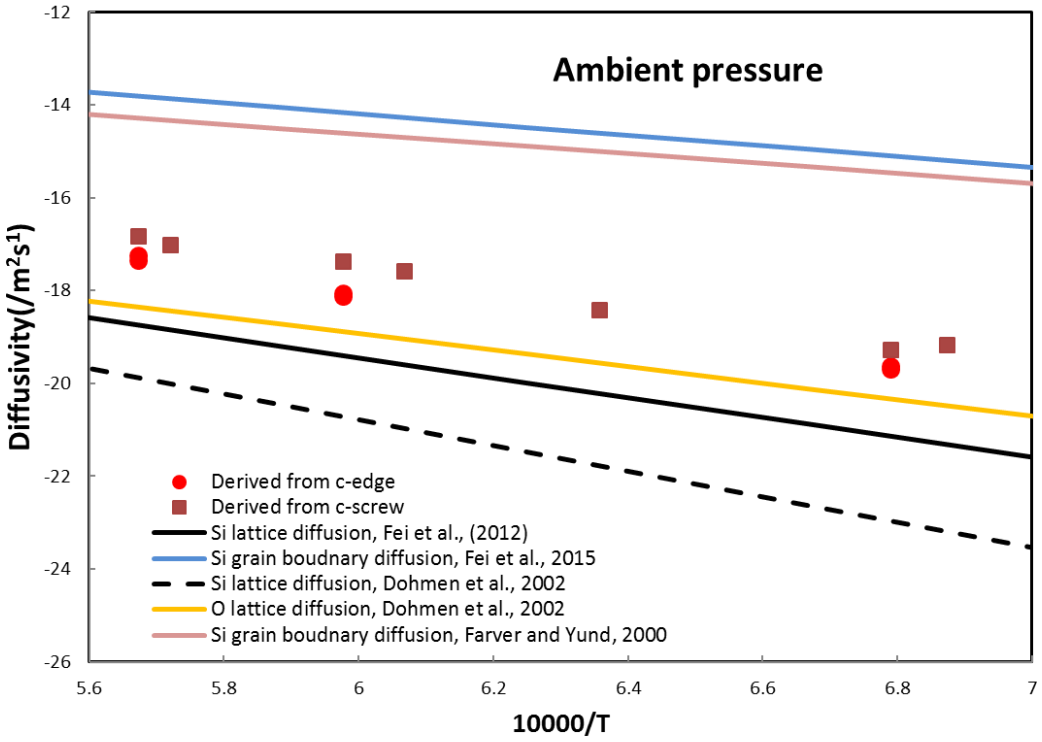

295